ACS Photonics

Article

pubs.acs.org/journal/apchd5

Terms of Use

Inhomogeneous Surface Plasmon Polaritons

Jonathan J. Foley, IV,[†] Jeffrey M. McMahon,[‡,§] George C. Schatz,[‡] Hayk Harutyunyan,[†] Gary P. Wiederrecht,[†] and Stephen K. Gray*[,†]

[†]Center for Nanoscale Materials, Argonne National Laboratory, Argonne, Illinois 60439, United States

[‡]Department of Chemistry, Northwestern University, Evanston, Illinois 60208, United States

[§]Department of Physics, University of Illinois at Urbana−Champaign, Urbana, Illinois 61801, United States

S *Supporting Information*

ABSTRACT: We show analytically and with rigorous computational electrodynamics how inhomogeneous surface plasmon polaritons (ISPPs) can be generated by refraction of ordinary SPPs at metal−metal interfaces. ISPPs, in contrast with SPPs, propagate and decay in different directions and can therefore exhibit significantly different intensity patterns. Our analytical arguments are based on a complex generalization of Snell's law to describe how SPPs moving on one metal surface are refracted at an interface with a second, different metal surface. The refracted waveform on the second metal is an ISPP. Under suitable circumstances the decay of an ISPP can be almost perpendicular to the propagation direction, leading to significant confinement. It is also found that ISPPs on the second metal can retain information about the SPPs on the first metal, a phenomenon that we term "dispersion imprinting". The complex Snell's law predictions are validated with 3-D finite-difference time-domain simulations, and possible means of experimentally observing ISPPs are suggested. The idea of ISPPs and how they result from refraction may expand the potential for designing the propagation and dispersion features of surface waves in general, including surface phonon polaritons, surface magnons, and guided waves in metamaterials.

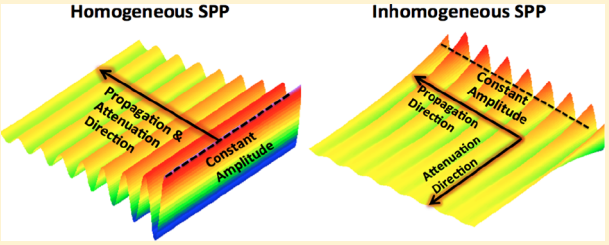

KEYWORDS: *plasmonics, surface waves, inhomogeneous waves, refraction, near-field optics, dispersion engineering*

Surface plasmon polaritons (SPPs) are surface waves created by coupling light into charge-density oscillations at a metal−dielectric interface that allow optical energy and information to be strongly confined to a two-dimensional surface.[1−7] Systems that permit the excitation of SPPs can exhibit interesting and unexpected optical properties, including extraordinary optical transmission[8] and superlensing.[9−11] Such properties are relevant to a wide range of applications including imaging and sensing[12−16] and optoelectronics,[17−20] so controlling and manipulating SPP propagation is a major goal of nanophotonics research.[21,22]

Because SPPs are exponentially confined both above and below a surface, one can attempt to describe their motion using classical optics ideas applied to the 2-D propagation plane. SPPs have been shown experimentally to exhibit refraction behavior when they propagate across an interface between two metal/dielectric interfaces with differing optical properties.[23,24] Negative refraction of SPP-dominated waveguide modes has also been achieved.[25] In this article, we analyze SPP refraction, presenting and discussing implications of a complex generalization of Snell's law to describe how SPPs propagating on one metal surface are refracted at an interface with a second, different metal surface. We find that the refracted waveform on the second metal surface is an inhomogeneous wave, which we term an inhomogeneous surface plasmon polariton (ISPP). The characteristic feature of an ISPP is that its lines of constant phase and amplitude are nonparallel; that is, its propagation and decay directions are different. By contrast, ordinary SPPs are homogeneous waves in the 2-D plane and are attenuated exactly along their direction of propagation. (Of course ordinary SPPs are evanescent above and below the metal surface, i.e., perpendicular to their propagation direction, and in this sense are trivially inhomogeneous.) We find that refraction can be exploited to introduce significant confinement in ISPPs without sacrificing propagation length. ISPPs propagating on the second metal surface also exhibit properties that depend on the angle of incidence and optical properties of SPPs on the first metal surface. For example, ISPPs on the second metal can exhibit different dispersion relations than ordinary SPPs on that same metal. These dispersion relations can actually exhibit features of the dispersion relations of ordinary SPPs on the first metal surface. We term this effect "dispersion imprinting" since, for example, the dispersion relation of an ISPP on an aluminum surface, arising from refraction of an SPP on a gold surface, can resemble the dispersion of ordinary SPPs on the gold surface. Importantly, dispersion imprinting can allow the extension of the SPP dispersion to frequencies higher than the ordinary back-bending frequency, for example, by the conversion of a radiative Brewster mode[6] into a bounded SPP mode.

Received: May 16, 2014
Published: July 23, 2014

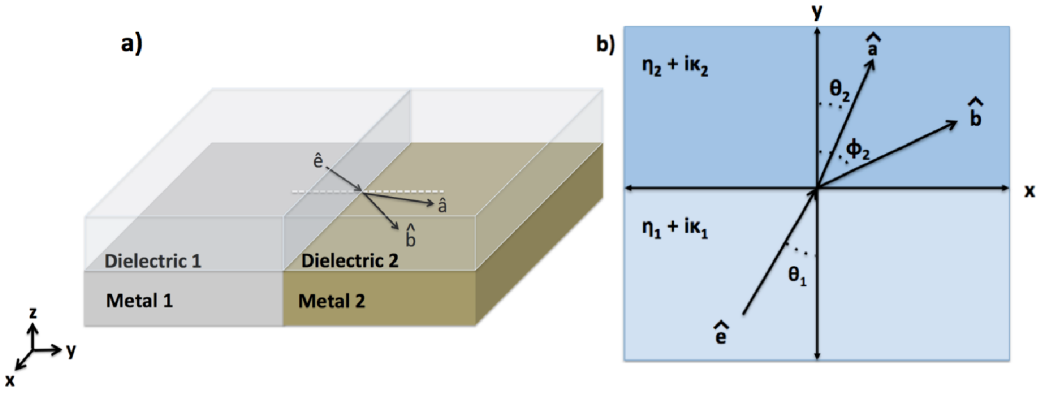

Figure 1. (a) Diagram of SPP refraction. The incident, ordinary SPP on metal 1 propagates with direction $\hat{\mathbf{e}}$ being associated with both the real and imaginary parts of its wavevector. The wavevector of the refracted ISPP on metal 2 has direction $\hat{\mathbf{a}}$ associated with its real part and direction $\hat{\mathbf{b}}$ associated with its imaginary part. (b) 2-D effective medium picture of the refraction in the $x-y$ plane of (a).

In the remainder of this article, we develop the theory of refraction of SPPs through a complex generalization of Snell's law (CSL). We show how this leads directly to the prediction of ISPPs with atypical waveforms and the ability to exhibit dispersion imprinting. We consider several concrete examples, verifying the analytical CSL predictions with rigorous electrodynamics simulations. Finally, we point to ways of experimentally observing ISPPs with leakage radiation microscopy.[26,27]

Refraction of 3-D plane waves in absorbing media has been considered by several authors.[28−33] Here we adapt the particularly transparent treatment of Chang, Walker, and Hopcraft[33] to the case of 2-D SPP refraction at the boundary between different metal surfaces. The system of interest involves an SPP propagating on metal surface 1 that has dielectric material 1 above it; it is reflected and refracted at the interface with a metal surface 2 with dielectric 2 above it (see Figure 1). The propagation of the SPPs on each surface can be described with 2-D waveforms moving in the $x-y$ plane of Figure 1,

$$\mathbf{E}_j = \mathbf{E}_{0,j} \exp(\mathrm{i}\mathbf{k}_j \cdot \mathbf{r} - \mathrm{i}\omega t) \tag{1}$$

where $\mathbf{k}_j$ is a complex SPP wavevector associated with incident ($j = 1$) or refracted ($j = 2$) waves. A 2-D medium refractive index may be defined based on the standard SPP dispersion relation:

$$\eta_j + \mathrm{i}\kappa_j = \left(\frac{\varepsilon_j \varepsilon_j^{\mathrm{D}}}{\varepsilon_j + \varepsilon_j^{\mathrm{D}}} \right)^{1/2} \tag{2}$$

where $\epsilon_j = \epsilon_j(\omega)$ is the frequency-dependent permittivity of metal j and ϵ_j^{D} is the permittivity of the dielectric material above it. While eq 2 assumes a semi-infinte metal bound by a semi-infinite dielectric, the following analysis is also valid for SPPs on finite films, where the medium refractive index may be inferred from calculation of multilayer waveguide modes.[34] The incident (ordinary) SPP wavevector is

$$\mathbf{k}_1 = \frac{\omega}{c}(\eta_1 + \mathrm{i}\kappa_1)\hat{\mathbf{e}} \tag{3}$$

where $\hat{\mathbf{e}} = \sin(\theta_1)\hat{x} + \cos(\theta_1)\hat{y}$ is a unit vector indicating the propagation direction. The lines of constant phase and amplitude for $\mathbf{E}_1$ are parallel and $\hat{\mathbf{e}}$ is normal to these lines, meaning $\mathbf{E}_1$ is a homogeneous wave. The refracted SPP (or ISPP) is allowed to be inhomogeneous: its lines of constant phase and amplitude are not necessarily parallel. The ISPP wavevector is thus assumed to be

$$\mathbf{k}_2 = \frac{\omega}{c}(N_2\hat{\mathbf{a}} + \mathrm{i}K_2\hat{\mathbf{b}}) \tag{4}$$

where $\hat{\mathbf{a}} = \sin(\theta_2)\hat{x} + \cos(\theta_2)\hat{y}$ is a unit vector normal to the lines of constant phase, $\hat{\mathbf{b}} = \sin(\phi_2)\hat{x} + \cos(\phi_2)\hat{y}$ is a unit vector normal to the lines of constant amplitude, and the effective indices N_2 and K_2 depend on refractive indices η_2, κ_2, η_1, and κ_1 and incident angle θ_1. The boundary conditions and wave equation determine N_2 and K_2 in terms of the known quantities. The SPP phases $\mathbf{k}_j \cdot \mathbf{r}$ must be continuous at the $y = 0$ interface, implying

$$\eta_1 \sin(\theta_1) = N_2 \sin(\theta_2) \tag{5}$$

$$k_1 \sin(\theta_1) = K_2 \sin(\phi_2) \tag{6}$$

We refer to eqs 5 and 6 as a complex generalization of Snell's law because they determine the angles of refraction of the real and imaginary parts of the ISPP wavevector. To determine N_2 and K_2, inserting $\mathbf{E}_2$ of the form eq 1 into the usual second-order electromagnetic wave equation gives

$$(\mathbf{k}_2 \cdot \mathbf{k}_2)\mathbf{E}_2 = \frac{\omega^2}{c^2}(\eta_2 + \mathrm{i}\kappa_2)^2 \mathbf{E}_2 \tag{7}$$

which is satisfied if

$$N_2^2 - K_2^2 = \eta_2^2 - \kappa_2^2 \tag{8}$$

and

$$N_2 K_2 \cos(\theta_2 - \phi_2) = \eta_2 \kappa_2 \tag{9}$$

Using eqs 5 and 6, eq 9 is equivalent to

$$\eta_2\kappa_2 - \alpha_1\beta_1 = \sqrt{N_2^2 - \alpha_1^2}\sqrt{N_2^2 - (\eta_2^2 - \kappa_2^2) - \beta_1^2} \tag{10}$$

where $\alpha_1 = \eta_1 \sin(\theta_1)$ and $\beta_1 = \kappa_1 \sin(\theta_1)$. Squaring both sides of eq 10 gives a quartic equation for N_2, which has one physical (positive real) solution,

$$N_2 = \frac{1}{\sqrt{2}}\sqrt{a + \sqrt{b}} \tag{11}$$

where

$$a = \alpha_1^2 + \beta_1^2 + \eta_2^2 - \kappa_2^2$$

dx.doi.org/10.1021/ph500172f | ACS Photonics 2014, 1, 739−745

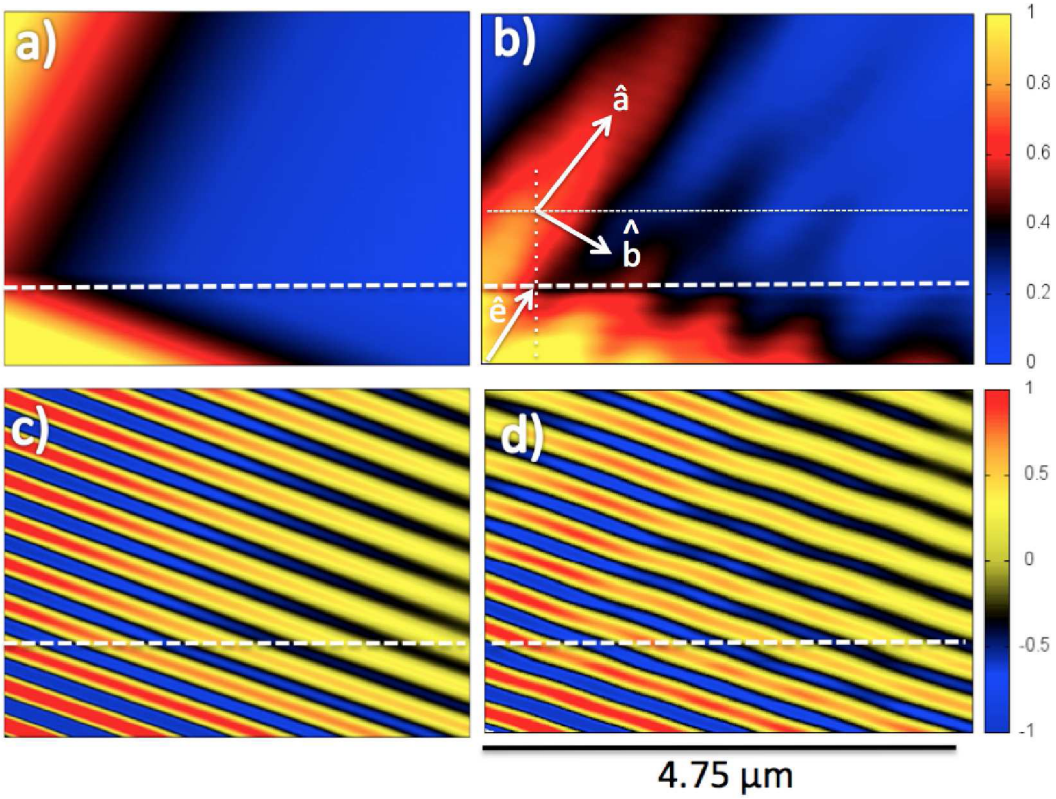

Figure 2. Field profiles of incoming SPP (below white dashed line) excited on Au by 532 nm light with $\theta_1 = 25°$ refracting onto an Ag surface (above white dashed line). Air is assumed to be above both surfaces. (a and b) Analytical (CSL) and FDTD electric field intensities, respectively. (c and d) Analytical and FDTD instantaneous electric field components, respectively. The FDTD results are x−y cuts taken at a z level 120 nm above metal surfaces and are associated with the z component of the electric field. The propagation and decay direction of the incident SPP is denoted by the vector $\hat{\mathbf{e}}$, the propagation direction of the ISPP is denoted by the vector $\hat{\mathbf{a}}$, and the decay direction of the ISPP is denoted by the vector $\hat{\mathbf{b}}$ in panel (b).

$$b = ((\kappa_2 - \beta_1)^2 + (\eta_2 - \alpha_1)^2)((\kappa_2 + \beta_1)^2 + (\eta_2 + \alpha_1)^2)$$

Once N_2 is known, K_2 may be determined readily using eq 8; θ_2 and ϕ_2 are then found from the CSL, eqs 5 and 6.

For normal incidence ($\theta_1 = 0$) the CSL leads to $N_2 = \eta_2$, $K_2 = \kappa_2$, and $\theta_2 = \phi_2$, i.e., a refracted SPP in medium 2 that is an ordinary SPP; otherwise, there are two new features. The first new feature is that $\theta_2 \neq \phi_2$, which is to say the waveform is inhomogeneous, meaning it loses amplitude along a different direction than its propagation direction. This property can introduce lateral confinement to an ISPP. The second new feature is that $N_2 \neq \eta_2$ and $K_2 \neq \kappa_2$; that is, the medium 2 ISPP refractive index components and, thus, dispersion are not the same as those for an ordinary SPP in medium 2. In fact, eq 11 implies that ISPP dispersion curves contain information about the angle of incidence of the medium 1 SPP, as well as the medium 1 dispersion. This represents a kind of memory effect, which we term dispersion imprinting. A similar memory effect is known to occur when ordinary 3-D waves in a dielectric medium are refracted into an absorbing medium.[30] We will also see that the values of N_2 and K_2 both can be larger than those for ordinary SPPs, where the former implies that the ISPP can have smaller wavelengths and greater momentum than an analogous ordinary SPP. Importantly, while K_2 is often larger than κ_2, the propagation length of the ISPP will not be shorter than the analogous ordinary SPP, but can show significant lateral confinement related to the magnitude of K_2.

The ISPP propagation length (L_P) is the distance, measured along the propagation direction, that the ISPP propagates when the intensity decays to $|\mathbf{E}|_0^2/e$. For an ordinary (homogeneous) SPP in medium 2, $L_P = 1/(2k_0\kappa_2)$, where k_0 is the free-space wavevector of the exciting light; $k_0 = 2\pi/\lambda_0$. For an ISPP, this distance is measured along $\hat{\mathbf{a}}$ and is given by $L_P = 1/(2k_0K_2 \cos(\theta_2 - \phi_2))$. Utilizing eq 9, the ratio of the ISPP propagation length to an ordinary SPP propagation length is simply N_2/η_2, and so if $N_2 > \eta_2$ there will be propagation length enhancement. We define a confinement length (L_C) as the distance in the direction perpendicular to propagation over which the ISPP intensity decays to $|\mathbf{E}|_0^2/e$, or $L_C = 1/(2k_0K_2 \sin(\theta_2 - \phi_2))$. A more confined SPP has a shorter confinement length. In the event of propagation length enhancement, K_2 itself will be larger than κ_2; hence propagation length enhancement can also be associated with strong confinement of the ISPP.

The above analysis concerns the form of the ISPP, which can be viewed as a refracted (or transmitted) wave. One can also consider appropriately adapted Fresnel equations for 2-D SPP propagation and infer reflection and transmission amplitudes in a manner similar to considerations of Chang and co-workers.[33] This allows one to estimate the efficiency of ISPP generation. See the Supporting Information for more information.

Consider Au for metal 1 and Ag for metal 2 with air as the dielectric above each metal, with an incident SPP excited on Au with $\lambda_0 = 532$ nm light. We take $\epsilon_1 = -4.762 + 2.378i$ and $\epsilon_2 = -11.825 + 0.374i$,[35] which gives medium refractive indices $\eta_1 = 1.092$, $\kappa_1 = 0.057$, $\eta_2 = 1.045$, and $\kappa_2 = 0.0015$. When $\theta_1 = 25°$ is considered, CSL predicts $\theta_2 = 26°$ and $\phi_2 = 112°$ (see Supporting Information, Figure S4; ϕ_2 can be larger than 90°).

dx.doi.org/10.1021/ph500172f | ACS Photonics 2014, 1, 739−745

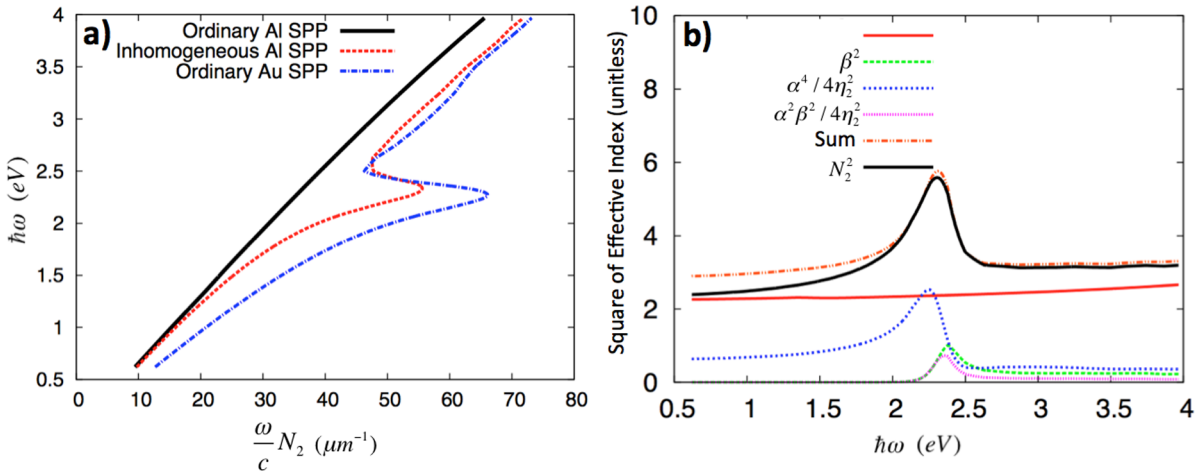

Figure 3. (a) Dispersion of the ISPP generated on aluminum (dashed red curve) by refraction of an ordinary gold SPP (dashed blue curve) compared to the dispersion of an ordinary aluminum SPP (black curve), illustrating a strong dispersion imprinting effect. (b) Plot of dominant terms in the approximate expansion of N_2^2 given in eq 12 for the Al ISPP dispersion.

The CSL electric field intensity, $|\mathbf{E}_z|^2$, and instantaneous field map, $\mathrm{Re}(\mathbf{E}_z)$, are shown in Figure 2a and c, respectively. To validate these predictions, we use rigorous 3-D finite-difference time-domain (FDTD) calculations[36,37] to simulate the refraction phenomena and plot $|\mathbf{E}_z|^2$ and $\mathrm{Re}(\mathbf{E}_z)$ in Figure 2b and d, respectively. (Other FDTD field components give similar results; see Supporting Information for more details on FDTD simulations.) The FDTD results show a high degree of similarity in the ISPP wavelength, propagation direction, and attenuation behavior with that predicted by CSL. Values of the simulated electric field intensity are sampled along the propagation direction ($\hat{\mathbf{a}}$) and fit an exponential to allow accurate inference of L_P (see Supporting Information, Figure S1). The FDTD fields do differ from the CSL ones in that there is a fast decay of the FDTD field in the upper left region of Figure 2b and d. This is simply due to the finite size of the excitation source used in the simulations (see Supporting Information). One can also see interference fringes in the FDTD results due to interference of incident and reflected waves.

The ISPP propagation length as determined by rigorous 3-D electrodynamics calculation is approximately 28 μm, compared to 27 μm from analytical predictions using the CSL. The FDTD instantaneous field allows us to infer a propagation direction of 27°, compared to the CSL prediction of 26°. It turns out that such propagation lengths (in this case) are not significantly different from those of ordinary SPPs on silver. However, there is significant lateral confinement compared to an ordinary SPP. We extract L_C, which is a measure of this confinement, by sampling the electric field intensity along the direction perpendicular to $\hat{\mathbf{a}}$. We find L_C of the ISPP is 1.1 μm as determined by FDTD calculation, which agrees closely with the CSL prediction of 1.7 μm (see Supporting Information, Figure S1). Note that an ordinary SPP in this medium would propagate with *no* such confinement lateral to the propagation direction. Analysis of the FDTD lines of constant amplitude allows us to infer an attenuation direction of 115°, similar to the CSL prediction of 112°. In this first example, ϕ_2 is much larger than θ_2; that is, the direction of the amplitude decay is nearly normal to the propagation direction. Regarding the effective indices in medium 2, it turns out that $K_2 = 0.0252$, which is significantly larger than the medium value of $\kappa_2 = 0.0015$, but that $N_2 \approx \eta_2 = 1.045$.

An additional example where SPPs excited on gold refract at an interface with aluminum is considered across a spectrum of frequencies to map out the dispersion of the resulting ISPP. Specifically, we consider SPPs excited on the surface of gold coated with TiO_2 that generate ISPPs by refraction at the interface with an aluminum surface coated with glass. We assume that $\epsilon_{TiO_2} = 4.0$ and $\epsilon_{Glass} = 2.25$. Here, the effects of dispersion imprinting are particularly evident, as the back-bending features of gold's dispersion are transferred to the plasmons propagating on aluminum, leading to a significant increase in N_2 relative to η_2 at moderate to large incident angles. Mapping out the real part of the propagation vector, $(\omega/c)N_2$, with $\theta_1 = 50°$ shows a startling departure from the ordinary Al/glass result (see Figure 3). The ordinary Al/glass dispersion is relatively featureless; the wavevector increases uniformly with ω. The dispersion of the ISPP shows markedly different features, including a dramatic slowing of group velocity in the frequency range between 1.5 and 2 eV and a back-bending region between 2 and 3 eV. These features mirror dispersion characteristics of SPPs on the gold/$\epsilon_2^D = 4$ medium (see Figure S3). To see the relationship between the details of the incident SPP and the dispersion of the ISPP more clearly, we note that η_2^4 can be factored out of b in eq 11 so the root can be written as $N_2 = {}^1/_2(a + \eta_2^2(1+f)^{1/2})^{1/2}$. Expanding $(1+f)^{1/2}$ to first order gives

$$N_2^2 \approx \eta_2^2 + \beta_1^2 - \frac{2}{\eta_2}\alpha_1\beta_1\kappa_2 + \frac{1}{4\eta_2^2}(\alpha_1^4 + \beta_1^4 + \kappa_2^4 + 2(\kappa_2^2\alpha_1^2 - \kappa_2^2\beta_1^2 + \beta_1^2\alpha_1^2)) \quad (12)$$

It is interesting to note that the terms involving α_1 (β_1) can make strong contributions to N_2 when θ_1 is large and η_1 (κ_1) is large. Both η_1 and κ_1 tend to be large in the vicinity of the surface plasmon resonance (SPR) of material 1, which in terms of the SPP dispersion is associated with the back-bending or anomalous dispersion region[6] (see Figure 3). Back-bending features can be encoded from material 1 to material 2 in general, but they will often be associated with high loss. Recalling the definitions of L_P and L_C, we observe that any additional loss imparted by refraction leads to greater

dx.doi.org/10.1021/ph500172f | ACS Photonics 2014, 1, 739−745

confinement of the ISPP and not additional attenuation in the propagation direction. We illustrate a particular refraction using 780 nm light and an incident angle of 50° that leads to a phenomenon that resembles total internal reflection (see Supporting Information, Figure S2). In fact, TIR-like refraction of SPPs has been experimentally demonstrated in other works.[23,24] The TIR-like ISPP can be thought of as an opposite extreme of the ISPP generated by refraction of the gold SPP onto silver at 532 nm illustrated in Figure 2. The SPP illustrated in Figure 2 has a small value for θ_2 and a large value of ϕ_2, whereas an SPP near the TIR extreme has a large value of θ_2 and a small value of ϕ_2. Because of the frequency dependence of η and κ, one can achieve a multitude of refraction scenarios spanning these extremes for a single system of interfaced metals.

The coupling of light into SPPs at frequencies near or above the back-bending region in gold is extremely inefficient using standard Kretschmann–Raether excitation configurations, as can be seen with analytical calculation of the complex transmission amplitudes for thin gold films sandwiched between air and glass.[38] By contrast, SPPs can be excited on silver surfaces in this frequency regime with relatively high efficiency. We consider generating ISPPs on 50 nm thin gold films by refraction of efficiently generated SPPs on 50 nm silver films with an angle of incidence of 60 degrees over the spectral range from approximately 2 to 3 eV, which encompasses gold's back-bending region. The dispersions of ordinary SPPs on 50 nm silver and gold films in this energy regime are plotted in Figure 4 for comparison with the ISPP dispersion on the gold

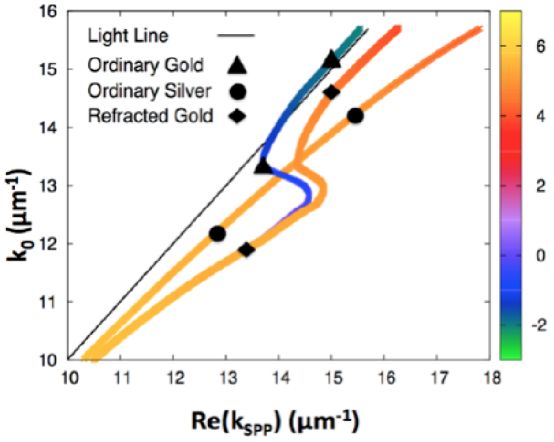

Figure 4. Dispersion of ordinary SPPs on silver, gold, and ISPPs on gold excited by ordinary SPPs on silver with an angle of incidence of 60°. Color coding indicates the natural log of the electric field intensity of SPPs calculated as described in the Supporting Information, Section 1.

film generated refraction of a silver SPP with an incident angle of 60 degrees. The dispersions of ordinary SPPs on 50 nm silver and gold films are inferred from the appropriate multilayer waveguide modes, calculated as described previously.[34] The dispersion curves are color-coded by the SPP electric field intensity for the ordinary SPPs and by the estimated ISPP intensity on the metal–metal boundary based on the transition probability (see Supporting Information Section 1). This illustrates several key points about the novelty of generating ISPPs by refraction. We can clearly see that the ordinary gold dispersion crosses the light line at approximately 2.8 eV, indicating that SPPs cannot be excited at or above this energy. Modes in this energy regime are termed Brewster modes and are not true surface waves.[6] In contrast, the ISPP gold dispersion does not cross the light line; hence the energy range of surface waves allowable on gold has been extended due to the effect of dispersion imprinting by the conversion of a Brewster mode to an ISPP mode.

Regarding experimental validation of the ISPP features we predict in this article, it is important to remember that ISPPs cannot be excited in the same manner as ordinary SPPs. Rather, such ordinary SPPs must be first generated, and it is their refraction at a metal–metal interface that creates ISPPs. Near-field optical microscopy (NSOM)[6] could be used to observe the unique intensity patterns of ISPPs generated in such a fashion, although there is always a concern about how the NSOM probe affects the field intensities, and such experiments can be time-consuming and challenging. We conclude by suggesting an experimentally simpler approach of observing ISPPs, based on leakage radiation,[26,27] that also allows for quantification of ISPP dispersions.

First consider the example of Kretschmann–Raether excitation of ordinary silver SPPs on the silver portion of a silver (metal 1)–gold (metal 2) SPP. We take the substrate to be glass (n = 1.5) and the dielectric above each metal to be air (n = 1). Light is incident on the metal surfaces from the glass below them, making an angle χ_1 with the normal to the metal surfaces. If χ_1 and the incident wavelength, $\lambda_0 = 2\pi/k_0$, are consistent with the momentum matching condition for silver SPPs, $1.5k_0 \sin(\chi_1 = \chi_{KR}) = k_0\eta_1$, then silver SPPs will be excited. (The observed reflectance back into the glass typically shows a strong dip as χ_1 passes through χ_{KR}.) Because gold and silver SPPs have very different dispersion relations, no ordinary gold SPPs will be created in this scenario. As the silver SPPs propagate, they leak radiation into the glass side, which can be observed in the far-field, with wavevectors directed along the same characteristic angle χ_{KR}; hence measuring the angle of the leakage radiation is analogous to measuring the SPP momentum.[26,27] These silver SPPs also refract at the metal–metal interface, generating ISPPs propagating on gold. The ISPPs will also emit leakage radiation but at an angle $\chi_2 = \sin^{-1}(N_2/1.5)$ characteristic of the ISPP dispersion. The angle χ_2 will, in general, be different from the angles associated with leakage radiation from ordinary silver or gold SPPs. Furthermore, this angle depends in a predictable way on the incident angle of the exciting SPP, θ_1, at the metal–metal interface. Note that ISPP leakage radiation is characterized by not only its out-of-plane angle, χ_2, but the in-plane refraction angle (arising from the CSL), θ_2.

The scenario described above is still experimentally challenging because ISPP leakage radiation will appear in a relatively small spot in 3-D space reflective of both χ_2 and θ_2 discussed above. (The finite-sized spot is due to the finite spatial width of the incident laser beam.) A simpler experimental approach, utilizing the same basic ideas, involves an oil immersion microscope objective positioned below the glass substrate and sample, which can be used both to excite ordinary SPPs and to collect the resulting reflected light and SPP and ISPP leakage radiation. Further details and an illustration of such an experiment are given in the Supporting Information.

We have shown that ISPPs can exhibit several unusual features, which were validated using 3-D electrodynamics simulations. In particular, the nature of ISPPs is that their propagation and decay directions are no longer the same as

dx.doi.org/10.1021/ph500172f | ACS Photonics 2014, 1, 739–745

they are for ordinary SPPs. It is then possible to introduce significant confinement that is almost perpendicular to the propagation direction. The ability to create these waveforms could have important impacts for advanced imaging applications, for instance, in providing lateral subdiffraction capabilities to technologies like total internal reflection fluorescence microscopy, which is currently capable of super-resolution only in the axial dimension.[39] A further consequence is that the ISPPs obey unique dispersion relations that depend on the supporting medium as well as the incident medium. We also suggested an experimental approach to observing ISPPs. The theory should be applicable to more complicated structures such as the layered waveguide modes described by Atwater and co-workers for the measurement of negative refraction in the visible spectrum;[25] such structures might provide an alternative for an experimentally realizable system for observing ISPPs. Although we do not discuss this application in detail, FDTD simulations demonstrate SPP focusing can be achieved using a metal region acting as a plasmonic lens (see Supporting Information, Figure S7). The focusing through refraction of such a lens could allow the generation of tightly confined and controlled SPP modes without loss of propagation length, which could also have applications both in super-resolution imaging and in optical information transfer. Optical switching devices could also be constructed using incident angle or superstrate dielectric constant as a knob to induce a dramatic change in the propagation behavior of the ISPP. Similarly, the unique dependence of the refracted wave on the dielectric properties of the incident medium may also prove useful in sensing applications.

Finally, we note that the ideas developed here could offer novel and powerful strategies for engineering the dispersions of surface waves in general. The CSL formulas derived herein are generally applicable or extendible to other guided waves with complex wavevectors traveling across heterogeneous surfaces. For example, such analysis could open up avenues for engineering the dispersion and propagation properties of surface phonon polaritons, guided surface modes in metamaterial structures, and surface magnons in materials with different magnetic domains.

■ ASSOCIATED CONTENT

Supporting Information

Transmission and reflection coefficients, propagation and confinement lengths, proposed experimental validation, and further details of the calculations and simulation details are provided in the Supporting Information. This material is available free of charge via the Internet at http://pubs.acs.org.

■ AUTHOR INFORMATION

Corresponding Author

*E-mail: gray@anl.gov.

Notes

The authors declare no competing financial interest.

■ ACKNOWLEDGMENTS

This work was performed, in part, at the Center for Nanoscale Materials, a U.S. Department of Energy, Office of Science, Office of Basic Energy Sciences User Facility, under Contract No. DE-AC02-06CH11357. J.M.M. and G.C.S. were supported by the Department of Energy, Office of Basic Energy Sciences, under grant DE-FG02-10ER16153. J.M.M. was also supported by the Department of Energy under grant DE-NA0001789.

■ REFERENCES

(1) Barnes, W.; Dereux, A.; Ebbesen, T. Surface plasmon subwavelength optics. *Nature* **2003**, *424*, 824−830.
(2) Zayats, A.; Smolyaninov, I.; Maradudin, A. Nano-optics of surface plasmon polaritons. *Phys. Rep.* **2005**, *408*, 131−314.
(3) Gramotnev, D. K.; Bozhevolnyi, S. I. Plasmonics beyond the diffraction limit. *Nat. Photonics* **2010**, *4*, 83−91.
(4) Stockman, M. I. Nanoplasmonics: past, present, and glimpse into future. *Opt. Express* **2011**, *19*, 22029−22106.
(5) Berini, P.; De Leon, I. Surface-plasmon polariton amplifiers and lasers. *Nat. Photonics* **2012**, *6*, 16−24.
(6) Novotny, L.; Hecht, B. *Principles of Nano-optics*, 2nd ed.; Cambridge University Press, 2012.
(7) Gray, S. K. Theory and modeling of plasmonic structures. *J. Phys. Chem. C* **2013**, *117*, 1983−1994.
(8) Ebbesen, T. W.; Lezec, H. J.; Ghaemi, H. F.; Thio, T.; Wolff, P. A. Extraordinary optical transmission through sub-wavelength hole arrays. *Nature* **1998**, *391*, 667−669.
(9) Pendry, J. B. Negative refraction makes a perfect lens. *Phys. Rev. Lett.* **2000**, *85*, 3966−3969.
(10) Fang, N.; Lee, H.; Sun, C.; Zhang, X. Sub-diffraction-limited optical imaging with a silver superlens. *Science* **2005**, *308*, 534−537.
(11) Stockman, M. I. Criterion for negative refraction with low optical losses from fundamental principle of causality. *Phys. Rev. Lett.* **2007**, *98*, 177404−177408.
(12) McMahon, J. M.; Henzie, J.; Odom, T. W.; Schatz, G. C.; Gray, S. K. Tailoring the sensing capabilities of nanohole arrays in gold films with Rayleigh anomaly-surface plasmon polaritons. *Opt. Express* **2007**, *15*, 18119−18129.
(13) Gao, H.; McMahon, J. M.; Lee, M. H.; Henzie, J.; Gray, S. K.; Schatz, G. C.; Odom, T. W. Rayleigh anomaly-surface plasmon polariton resonances in palladium and gold subwavelength hole arrays. *Opt. Express* **2009**, *17*, 2334−2340.
(14) Stewart, M. E.; Anderton, C. R.; Thompson, L. B.; Maria, J.; Gray, S. K.; Rogers, J. A.; Nuzzo, R. G. Nanostructured plasmonic sensors. *Chem. Rev.* **2008**, *108*, 494−521.
(15) Homola, J. Surface plasmon resonance sensors for detection of chemical and biological species. *Chem. Rev.* **2008**, *108*, 462−493.
(16) Swiontek, S. E.; Pulsifer, D. P.; Lakhtakia, A. Optical sensing of analytes in aqueous solutions with a multiple surface-plasmon-polariton-wave platform. *Sci. Rep.* **2013**, *3*, 1409−1414.
(17) Ozbay, E. Plasmonics: merging photonics and electronics at nanoscale dimensions. *Science* **2006**, *113*, 189−193.
(18) Zhang, J.; Zhang, L.; Xu, W. Sufrace plasmon polaritons: physics and applications. *J. Phys. D Appl. Phys.* **2012**, *45*, 113001−113020.
(19) Paul, A.; Solis, Jr.; Bao, K.; Chang, W.-S.; Nauert, S.; Vidgerman, L.; Zubarev, E. R.; Nordlander, P.; Link, S. Identification of higher order long-propagation-length surface plasmon polariton modes in chemically prepared gold nanowires. *ACS Nano* **2012**, *6*, 8105−8113.
(20) Saleh, A.; Dionne, J. Waveguides with a silver lining: low threshold gain and giant modal gain in cylindrical and coaxial plasmon slot waveguides. *Phys. Rev. B* **2012**, *85*, 045407−045419.
(21) Huidobro, P. A.; Nesterov, M. L.; Martin-Moreno, L.; García-Vidal, F. J. Transformation optics for plasmonics. *Nano Lett.* **2010**, *10*, 1985−1990.
(22) Pendry, J. B.; Aubry, A.; Smith, D. R.; Maier, S. A. Transformation optics and subwavelength control of light. *Science* **2012**, *337*, 549−552.
(23) Kitazawa, T.; Miyanishi, S.; Murakami, Y.; Kojima, K.; Takahashi, A. Refraction of surface plasmon-polaritons at Au-Al boundaries observed by scanning near-field optical microscopy. *Phys. Rev. B* **2008**, *77*, 193404.
(24) Griesing, S.; Englisch, A.; Hartmann, U. Refractive and reflective behavior of polymer prisms used for surface plasmon guidance. *Opt. Lett.* **2008**, *33*, 575−577.

(25) Lezec, H. J.; Dionne, J. A.; Atwater, H. A. Negative refraction at visible frequencies. *Science* **2007**, *316*, 430−432.
(26) Bouhelier, A.; Wiederrecht, G. P. Excitation of broadband surface plasmon polaritons: plasmonic continuum spectroscopy. *Phys. Rev. B* **2005**, *71*, 195406.
(27) Drezet, A.; Hohenau, A.; Koller, D.; Stepanov, A.; Ditlbacher, H.; Steinberger, B.; Aussenegg, F. R.; Leitner, A.; Krenn, J. R. Leakage radiation microscopy of surface plasmon polaritons. *Mater. Sci. Eng., B* **2008**, *149*, 220−229.
(28) Ciddor, P. E. Refraction into an absorbing medium. *Am. J. Phys.* **1976**, *44*, 786.
(29) Parmigiani, F. Some aspects of the reflection and refraction of an electromagnetic wave at an absorbing surface. *Am. J. Phys.* **1982**, *51*, 245−247.
(30) Born, M.; Wolf, E. *Principles of Optics*, 7th ed.; Cambridge Univ. Press: Cambridge, UK, 2002.
(31) Mahan, A. I. Reflection and refraction at oblique incidence on a dielectric-metallic interface as a boundary value problem in electromagnetic theory. *J. Opt. Soc. Am.* **1956**, *46*, 913−926.
(32) Dupertuis, M. A.; Proctor, M.; Acklin, B. Generalization of complex Snell-Descartes and Fresnel laws. *J. Opt. Soc. Am.* **1994**, *11*, 1159−1166.
(33) Chang, P. C. Y.; Walker, J. G.; Hopcraft, K. I. Ray tracing in absorbing media. *J. Quant. Spectrosc. Radiat. Transfer* **2005**, *96*, 327−341.
(34) Montgomery, J. M.; Gray, S. K. Enhancing surface plasmon polariton propagation lengths via coupling to asymmetric waveguide structures. *Phys. Rev. B* **2008**, *77*, 125407−125415.
(35) Johnson, P. B.; Christy, R. W. Optical constants of noble metals. *Phys. Rev. B* **1972**, *6*, 4370.
(36) Taflove, A.; Hagness, S. C. *Computational Electrodynamics: The Finite-Difference Time-Domain Method*; Artech, 2000.
(37) Montgomery, J. M.; Lee, T.-W.; Gray, S. K. Theory and modeling of light interactions with metallic nanostructures. *J. Phys.: Conds. Matter* **2008**, *20*, 323201−323222.
(38) Raether, H. *Surface Plasmons on Smooth and Rough Surfaces and on Gratings*; Springer-Verlag, 1988.
(39) Schermelleh, L.; Heintzmann, R.; Leonhardt, H. A guide to super-resolution fluorescence microscopy. *J. Cell Biol.* **2010**, *190*, 165−175.